A Frictionless Bristle-Based Friction Model That Exhibits Hysteresis and the Dynamic Stribeck Effect[☆]

Bojana Drinčić[a,*], Dennis S. Bernstein[a]

[a]*Department of Aerospace Engineering, The University of Michigan, Ann Arbor, MI 48109-2140, (734) 764-3719, (734) 763-0578 (FAX)*

Abstract

In this paper we investigate the origin of the Stribeck effect. We develop an asperity-based friction model and show that the vertical motion of a sliding body leads to a dynamic Stribeck effect. The friction model is hysteretic, and the energy-dissipation mechanism is the sudden release of the compressed bristles. We relate this model to the LuGre model.

Keywords: friction, hysteresis, stick-slip, Stribeck effect, bristle model, LuGre model

1. Introduction

Friction is a widespread phenomenon in many control and modeling applications as well as in everyday life [1–3]. Too little friction can be hazardous, while too much friction wastes energy. In both cases, a better understanding of friction is essential for improved design, analysis, and prediction.

Experimental observations provide the primary approach to understanding how friction depends on material properties and the relative motion between the contacting surfaces [4–6]. For example, the classic paper [4] measures the effect of relative speed, contact pressure, and surface separation on the friction force. Experimental observations lead to the development of

[☆]This research was made with Government support under and awarded by DoD, Air Force Office of Scientific Research, National Defense Science and Engineering Graduate (NDSEG) Fellowship, 32 CFR 168a and NSF grant 0758363.

[*]Corresponding author

Email addresses: bojanad@umich.edu (Bojana Drinčić), dsbaero@umich.edu (Dennis S. Bernstein)

empirical models that capture the macroscopic properties of friction [2, 7–13]. The LuGre model captures stick-slip friction when a sliding object is connected to a stiffness. The LuGre model also exhibits the Stribeck effect [9, 11], which predicts a drop in the friction force as the speed increases.

The approach we take to modeling friction is neither experimental nor empirical, but rather is motivated by asperity-based mechanistic models [14–17], in which the asperities represent the microscopic roughness of the contacting surfaces. In this conceptual approach, the goal is to postulate a model consisting of many degrees of freedom (for example, bristle deflections), where each component has precisely defined mechanical properties. The analysis and simulation of this model then gives rise to an emergent macroscopic friction force whose properties can be traced back to the properties of the components.

An advantage of this approach is that the hysteretic energy-dissipation mechanism is exposed. For example, in the compressed bristle model presented here, energy dissipation at asymptotically low frequency [18] is due to the sudden release of the compressed bristles, just as in the rotating bristle model discussed in [19, 20]. As the body encounters each bristle, energy is stored in the compressed spring and is subsequently dissipated by the dashpot due to the post-release oscillation of the bristle. Although the LuGre model [13] is hysteretic, the hysteretic mechanism is not exposed. Additionally, since the bristles represent the asperities of the contacting surface, the compression of the bristles is analogous to plastic deformation of the asperities, which also results in the loss of energy.

The goal of the present paper is to construct a bristle model that exhibits both stick-slip behavior and the Stribeck effect. Stick-slip behavior is exhibited by the rotating bristle model given in [19, 20]; however, the Stribeck effect was not found to be a property of that model.

The Stribeck effect is the apparent drop in the friction force as the velocity increases. In wet friction, the Stribeck effect can be attributed to the phenomenon of *planing* [21–23], where the friction between a tire and a wet surface decreases with velocity, resulting in a dangerous situation. For a boat on water, the same phenomenon is more apparent since the boat rises as its speed increases, thus reducing its contact area, which in turn reduces the drag due to the water, that is, the viscous friction force. For a vehicle immersed in a fluid, such as an aircraft, however, we would not expect to see the Stribeck effect. The Stribeck effect thus depends on contact at the boundary of a fluid and motion orthogonal to the surface of the fluid.

In modeling dry friction, which is the objective of a bristle model, it seems plausible in analogy with wet friction that the Stribeck effect would be observed as long as the body posesses a vertical degree of freedom. In particular, by extending the bristle model in [19, 20] to include a vertical degree of freedom, we would expect to observe the Stribeck effect due to the fact that the moment arm is increased—and thus the friction force is decreased—as the height of the mass above the contacting surface increases.

Rather than revisit the rotating bristle model of [19, 20], in the present paper we develop an alternative bristle model in which each bristle has a vertical degree of freedom rather than a rotational degree of freedom. This model gives rise to the Stribeck effect. Somewhat surprisingly, and unlike the Stribeck effect captured empirically by the LuGre model [19, 20], the Stribeck effect captured by this bristle model is dynamic in the sense that the speed/friction-force curve forms a loop. We call this the *dynamic Stribeck effect*.

The contents of the paper are as follows. In Section 2 we introduce the compressed bristle model, derive the governing equations, and show that the compressed bristle model exhibits stick-slip, hysteresis, and the dynamic Stribeck effect. Based on the observations in Section 2, we capture the steady-state characteristics of the compressed bristle model in the form of a single-state friction model in Section 3. We show that a simplified version of the compressed bristle model is equivalent to the LuGre model.

2. Compressed Bristle Model

In this section we present the compressed bristle model, which is based on the frictionless contact between a body and a row of bristles. The friction force of the bristle model is generated through the frictionless interaction between a body and bristles as shown in Figure 1. We assume that the body has mass m, length d, and thickness w, and that its front end is slanted from the vertical by the angle α. The body is allowed to move in the horizontal and vertical directions, but it does not rotate. The horizontal position of the midline of the body is denoted by x, and the vertical position of the midline of the body is denoted by y. The bristles consist of a frictionless roller, a spring with stiffness coefficient k, and a dashpot with damping coefficient c. The damping coefficient provides viscous energy dissipation but negligible force. The mass of the roller is assumed to be negligible compared to the mass of the body. Therefore, the interaction between each bristle and the

body is dominated by the stiffness of the bristle. The distance between adjacent bristles is Δ, the position of the ith bristle is denoted by x_{b_i}, and its length is h_i. Each bristle has length h_0 when relaxed. As the body moves, the bristles are compressed, which results in a reaction force at the point of contact between the bristle and the body. The friction force is the sum of all horizontal components of the forces exerted by all of the bristles contacting the slanted surface of the body. The vertical components of the forces exerted by the bristles contacting the body affect the vertical motion of the body.

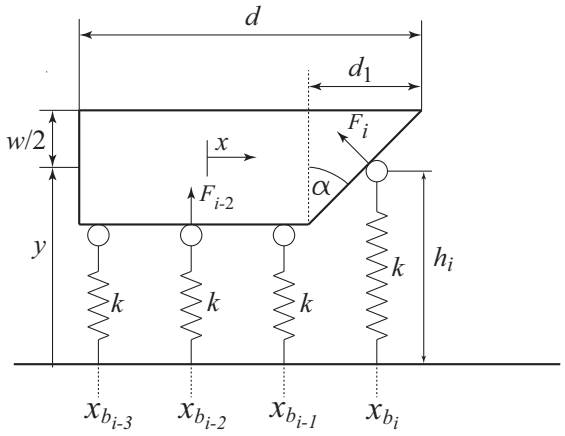

Figure 1: Schematic representation of the compressed bristle model. Each bristle consists of a frictionless roller of negligible mass, a linear spring with stiffness coefficient k, and a dashpot with damping coefficient c (not shown). As the body moves over the bristles, the bristle springs are compressed, and a reaction force occurs at the point of contact between each roller and the body.

As the body moves, there is a frictionless reaction force between each bristle and the body at the point of contact. This force is due to the compression of the bristle. We assume that the force on the body due to contact with the bristle is perpendicular to the surface of the body. The sum of all horizontal forces exerted by the bristles at each instant is defined to be the friction force. Since the bristle-body contact is frictionless, the direction of the reaction force between the body and each bristle contacting the horizontal surface of the body is vertical, and thus these bristles do not contribute to the friction force. Only the bristles that are in contact with the slanted surface of the body contribute to the friction force.

The force between the body and each bristle is calculated based on the position of the bristle relative to the body and the resulting length of the compressed bristle. The reaction forces due to the dashpot are neglected. The dashpots and mass of the bristles provide the mechanism for dissipating the energy stored in the compressed springs, but otherwise play no role in the bristle-body interactions.

In simulations of the bristle model we assign numerical values to the bristle-related parameters, such as Δ and k. However, these values do not necessarily represent physically meaningful quantities, but rather serve only to illustrate the interaction between the body and the asperities.

2.1. Friction Force

In this section we analyze the interaction between the body and the bristles, and we derive equations for the friction force of the compressed bristle model. For simplicity, we assume that at the instant the velocity of the body passes through zero, the body instantaneously rotates about the vertical axis that defines the horizontal position x of the body, so that its slanted surface always points in the direction of motion and such that x and y remain constant during the direction reversal.

The length h_i of the ith bristle contacting the slanted surface of the body is a function of the horizontal position x and velocity v of the body as described by

$$h_i(x, v, y) \triangleq \begin{cases} h_{i+}(x, y), \, v \geq 0, \\ h_{i-}(x, y), \, v < 0, \end{cases} \tag{1}$$

where

$$h_{i+}(x, y) = y - \frac{w}{2} + \frac{w}{d_1}\left(x_{b_i} - \left(x + \frac{d}{2} - d_1\right)\right), \tag{2}$$

$$h_{i-}(x, y) = y - \frac{w}{2} + \frac{w}{d_1}\left(x - \frac{d}{2} + d_1 - x_{bi}\right), \tag{3}$$

and $d_1 \triangleq w \tan(\alpha)$ as shown in Figure 1. The magnitude of the force due to the ith bristle is

$$F_i(x, v, y) = k(h_0 - h_i(x, v, y)). \tag{4}$$

The magnitude of the horizontal component of the reaction force due to the ith bristle is

$$F_{ix}(x, v, y) = k\cos(\alpha)(h_0 - h_i(x, v, y)), \tag{5}$$

while the magnitude of the vertical component of reaction force due to the ith bristle is

$$F_{iy}(x, v, y) = k\sin(\alpha)(h_0 - h_i(x, v, y)). \tag{6}$$

The friction force is the sum of all of the horizontal components of the reaction forces between the bristles and the body. Only the bristles that are in contact with the slanted surface of the body exert a force with a horizontal component. The base positions x_{b_i} of the bristles that contribute to the friction force for $v \geq 0$ are in the set

$$\mathcal{X}_{b+}(x) = \{x_{b_i} : x + \frac{d}{2} - d_1 \leq x_{b_i} \leq x + \frac{d}{2}\}, \tag{7}$$

and, for $v < 0$, are in the set

$$\mathcal{X}_{b-}(x) = \{x_{b_i} : x - \frac{d}{2} \leq x_{b_i} \leq x - \frac{d}{2} + d_1\}. \tag{8}$$

Thus, for $v \geq 0$, the friction force is

$$F_f(x, v, y) = F_{f+}(x, y), \tag{9}$$

where

$$F_{f+}(x, y) = k\cos(\alpha)\sum_{i=1}^{n_+}(h_0 - h_{i+}(x, v, y)), \tag{10}$$

and n_+ is the number of elements of $\mathcal{X}_{b+}(x)$. For $v < 0$, the friction force is

$$F_f(x, v, y) = F_{f-}(x, y), \tag{11}$$

where

$$F_{f-}(x,y) = -k\cos(\alpha)\sum_{i=1}^{n_-}(h_0 - h_{i-}(x,v,y)), \tag{12}$$

where n_- is the number of elements of $\mathcal{X}_{b-}(x)$. Expressions (9) and (11) can be combined, so that $F_f(x,v,y)$ is given by

$$F_f(x,v,y) = \text{sign}(v)k\cos(\alpha)\sum_{i=1}^{n}(h_0 - h_i(x,v,y)), \tag{13}$$

where n is the number of elements of $\mathcal{X}_{b+}(x)$ for $v \geq 0$ and of $\mathcal{X}_{b-}(x)$ for $v < 0$. Note that, due to the function sign(v), (13) is discontinuous at $v = 0$.

The vertical force due to the bristles contacting the slanted surface of the body is equal to the sum of all of the vertical components of the reaction forces between the body and the bristles contacting the slanted surface of the body. We define the vertical force due to bristles contacting the slanted surface of the body as

$$F_{ys}(x,v,y) = \begin{cases} F_{ys+}(x,y),\ v \geq 0, \\ F_{ys-}(x,y),\ v < 0, \end{cases} \tag{14}$$

where

$$F_{ys+}(x,y) = k\sin(\alpha)\sum_{i=1}^{n_+}(h_0 - h_{i+}(x,v,y)), \tag{15}$$

$$F_{ys-}(x,y) = k\sin(\alpha)\sum_{i=1}^{n_-}(h_0 - h_{i-}(x,v,y)). \tag{16}$$

The magnitude of the vertical force due to the bristles contacting the horizontal surface of the body is

$$F_{yb}(y) = \sum_{i=1}^{N} k\left(h_0 - \left(y - \frac{w}{2}\right)\right) = Nk\left(h_0 - y + \frac{w}{2}\right), \tag{17}$$

where $N \triangleq \frac{d-d_1}{\Delta} + 1$ is the number of bristles that are in contact with the horizontal surface of the body.

2.2. Equations of motion

The goal is to investigate the stick-slip and input-output properties of the compressed bristle model. To investigate the emergence of stick-slip, we consider the system shown in Figure 2. The body of mass m is connected to a spring with stiffness K, and the free end of the spring moves at the constant speed v_p. The equations of motion describing the mass-spring system in Figure 2 are

$$\dot{x}(t) = v(t), \tag{18}$$

$$\dot{v}(t) = \frac{1}{m}(Kl(t) - F_f(x, v, y)), \tag{19}$$

$$\dot{l}(t) = v_p - v(t), \tag{20}$$

where l is the length of the spring and $F_f(x, v, y)$ is the friction force (13).

Since the compressed bristle model accounts for horizontal and vertical motion of the body, we augment (18)-(20) with vertical-direction equations of motion. The vertical motion of the body is described by

$$m\ddot{y} = -mg + F_y(x, v, y), \tag{21}$$

$$F_y(x, v, y) = F_{ys}(x, v, y) + F_{yb}(y), \tag{22}$$

where F_{ys} and F_{yb} are defined by (14) and (17), respectively. Note that (21)-(22) can be rewritten as

$$m\ddot{y}(t) + k_{uo}y(t) = f(t), \tag{23}$$

where, for $v \geq 0$, $k_{uo} = Nk + n_+ k \sin\alpha$ and

$$f = Nk(h_0 + \frac{w}{2}) - mg + k\sin\alpha \sum_{i=1}^{n_+} \left(h_0 + \frac{w}{2} - \frac{w}{d_1}\left(x_{b_i} - x - \frac{d}{2} + d_1 \right) \right), \tag{24}$$

and, for $v < 0$, $k_{uo} = Nk + n_- k \sin\alpha$ and

$$f = Nk(h_0 + \frac{w}{2}) - mg \\ + k\sin\alpha \sum_{i=1}^{n_-} \left(h_0 + \frac{w}{2} - \frac{w}{d_1}\left(x - \frac{d}{2} + d_1 - x_{b_i} \right) \right). \qquad (25)$$

Thus (21)-(22) describe an undamped oscillator.

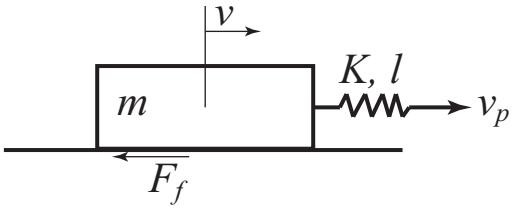

Figure 2: Schematic representation of the mass-spring system used to investigate the stick-slip properties of the bristle model. The body of mass m is connected to a spring with stiffness K. The free end of the spring moves at the constant speed v_p. The friction force F_f is given by (13).

To investigate the input-output properties and the emergence of hysteresis, we consider the mass-spring system shown in Figure 3. The body of mass m is connected to a wall by means of a spring with stiffness K and acted on by the force input $u(t)$. The equations of motion are

$$\dot{x}(t) = v(t), \qquad (26)$$

$$\dot{v}(t) = \frac{1}{m}(-Kx(t) + u(t) - F_f(x, v, y)), \qquad (27)$$

where $F_f(x, v, y)$ is the bristle model friction force (13). Furthermore, the vertical motion of the body is described by (21)-(22).

2.3. Switch Model

Due to the discontinuity of the bristle model friction force (13) at $v = 0$, numerical integration of (18)-(27) with the friction force represented by the compressed bristle model (13) requires special techniques. In this section we describe the Switch Model [24, 25], which is a technique that smooths

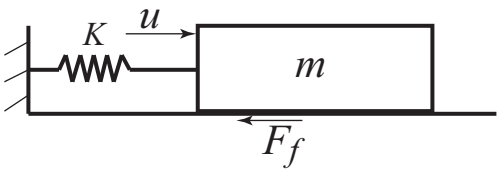

Figure 3: Body-spring configuration used to investigate the input-output properties of the bristle model. The body of mass m is connected to the wall by a means of a spring with stiffness K and is acted on by the force input $u(t)$. The friction force F_f is given by (13).

out the discontinuous dynamics around the discontinuity $v = 0$. The modified equations can then be integrated using standard numerical integration techniques.

To begin, we rewrite the equations of motion in which the friction force is modeled by the compressed bristle model as a differential inclusion [25]. Assume that the motion of the body is described by

$$\dot{\boldsymbol{x}} = \boldsymbol{f}(\boldsymbol{x}), \tag{28}$$

where $\boldsymbol{x} \in \mathbb{R}^m$, $\boldsymbol{f} : \mathcal{V} \subset \mathbb{R}^m \to \mathbb{R}^m$ is a piecewise continuous vector field, and $\Sigma \triangleq \mathbb{R}^m \backslash \mathcal{V}$ is the set of points of discontinuity of $\boldsymbol{f}$. We assume that there exists a function $g : \mathbb{R}^m \to \mathbb{R}$ such that the discontinuity boundary Σ is given by the roots of g, that is,

$$\Sigma = \{\boldsymbol{x} \in \mathbb{R}^m : \ g(\boldsymbol{x}) = 0\}. \tag{29}$$

We also define sets

$$\mathcal{V}_+ \triangleq \{\boldsymbol{x} \in \mathbb{R}^m : \ g(\boldsymbol{x}) > 0\}, \tag{30}$$

$$\mathcal{V}_- \triangleq \{\boldsymbol{x} \in \mathbb{R}^m : \ g(\boldsymbol{x}) < 0\}. \tag{31}$$

With these definitions, (28) can be rewritten as the differential inclusion [25, 26]

$$\dot{\boldsymbol{x}} \in \begin{cases} \boldsymbol{f}_+(\boldsymbol{x}), \ \boldsymbol{x} \in \mathcal{V}_+, \\ \alpha \boldsymbol{f}_+(\boldsymbol{x}) + (1-\alpha)\boldsymbol{f}_-(\boldsymbol{x}), \ \boldsymbol{x} \in \Sigma, \ \alpha \in [0,1], \\ \boldsymbol{f}_-(\boldsymbol{x}), \ \boldsymbol{x} \in \mathcal{V}_-. \end{cases} \tag{32}$$

The direction of flow given by the vector fields $\boldsymbol{f}_+(\boldsymbol{x})$ and $\boldsymbol{f}_-(\boldsymbol{x})$ can lead to three types of sliding modes across Σ. If the flow is such that the solutions of (32) are pushed to Σ from both $\mathcal{V}_+$ and $\mathcal{V}_-$, then the sliding mode is *attractive*. If the solutions cross Σ, then the sliding mode is *transversal*. Finally, if the solutions diverge from Σ, the sliding mode is *repulsive* [25].

The Switch Model smooths out the dynamics of the differential inclusion (32) by constructing a *stick band* within the set $\mathcal{G} \triangleq \{\boldsymbol{x} : |g(\boldsymbol{x})| \leq \eta\}$, where η is a small positive constant. (Note that the term "stick band" is not related to stick-slip friction.) The dynamics outside of the stick band remain the same. The dynamics inside the stick band depend on the type of sliding mode across the discontinuity boundary. If the sliding mode is attractive, that is,

$$\boldsymbol{n}^{\mathrm{T}}\boldsymbol{f}_-(\boldsymbol{x}) > 0 \,\text{and}\, \boldsymbol{n}^{\mathrm{T}}\boldsymbol{f}_+(\boldsymbol{x}) < 0, \quad \boldsymbol{x} \in \Sigma, \tag{33}$$

where $\boldsymbol{n} \triangleq \nabla g(\boldsymbol{x})$ is the normal to Σ, then the stick-band dynamics are given by

$$\dot{\boldsymbol{x}} = \alpha\boldsymbol{f}_+(\boldsymbol{x}) + (1-\alpha)\boldsymbol{f}_-(\boldsymbol{x})\,,\, \boldsymbol{x} \in \mathcal{G}. \tag{34}$$

The value of the parameter α is chosen such that it pushes the solutions of (33) toward the middle of the stick band, that is, toward $\{\boldsymbol{x} : g(\boldsymbol{x}) = 0\}$. Thus, inside the stick band, g satisfies

$$\dot{g}(\boldsymbol{x}) = -\tau g(\boldsymbol{x}), \tag{35}$$

where $\tau > 0$ is a time constant. Since

$$\dot{g}(\boldsymbol{x}) = \frac{dg(\boldsymbol{x})}{d\boldsymbol{x}}\frac{d\boldsymbol{x}}{dt} = \nabla\boldsymbol{g}^T\dot{\boldsymbol{x}} \tag{36}$$

$$= \boldsymbol{n}^T\left(\alpha\boldsymbol{f}_+(\boldsymbol{x}) + (1-\alpha)\boldsymbol{f}_-(\boldsymbol{x})\right), \tag{37}$$

setting (35) equal to (37) and solving for α gives

$$\alpha = \frac{\boldsymbol{n}^T\boldsymbol{f}_-(\boldsymbol{x}) + \tau^{-1}g(\boldsymbol{x})}{\boldsymbol{n}^T(\boldsymbol{f}_-(\boldsymbol{x}) - \boldsymbol{f}_+(\boldsymbol{x}))}. \tag{38}$$

If the sliding mode is transversal, that is,

$$(\boldsymbol{n}^{\mathrm{T}}\boldsymbol{f}_{-}(\boldsymbol{x}))(\boldsymbol{n}^{\mathrm{T}}\boldsymbol{f}_{+}(\boldsymbol{x})) > 0, \quad \boldsymbol{x} \in \Sigma, \tag{39}$$

then the stick-band dynamics are defined by

$$\dot{\boldsymbol{x}} = \begin{cases} \boldsymbol{f}_{-}(\boldsymbol{x}), \text{ if } \boldsymbol{n}^{\mathrm{T}}\boldsymbol{f}_{-}(\boldsymbol{x}) < 0 \text{ and } \boldsymbol{n}^{\mathrm{T}}\boldsymbol{f}_{+}(\boldsymbol{x}) < 0\,,\ \boldsymbol{x} \in \mathcal{G}, \\ \boldsymbol{f}_{+}(\boldsymbol{x}), \text{ if } \boldsymbol{n}^{\mathrm{T}}\boldsymbol{f}_{-}(\boldsymbol{x}) > 0 \text{ and } \boldsymbol{n}^{\mathrm{T}}\boldsymbol{f}_{+}(\boldsymbol{x}) > 0\,,\ \boldsymbol{x} \in \mathcal{G}. \end{cases} \tag{40}$$

Finally, if the sliding mode is repulsive, that is,

$$\boldsymbol{n}^{\mathrm{T}}\boldsymbol{f}_{-}(\boldsymbol{x}) < 0 \text{ and } \boldsymbol{n}^{\mathrm{T}}\boldsymbol{f}_{+}(\boldsymbol{x}) > 0, \quad \boldsymbol{x} \in \Sigma, \tag{41}$$

then the dynamics are defined by

$$\dot{\boldsymbol{x}} = \boldsymbol{f}_{+}(\boldsymbol{x})\,,\ \boldsymbol{x} \in \mathcal{G}. \tag{42}$$

Outside of the stick band, the dynamics are defined by

$$\dot{\boldsymbol{x}} = \begin{cases} \boldsymbol{f}_{+}(\boldsymbol{x}),\ \boldsymbol{x} \in \mathcal{G}_{+}, \\ \boldsymbol{f}_{-}(\boldsymbol{x}),\ \boldsymbol{x} \in \mathcal{G}_{-}, \end{cases} \tag{43}$$

where $\mathcal{G}_{+} \triangleq \{\boldsymbol{x} : g(\boldsymbol{x}) > \eta\}$ and $\mathcal{G}_{-} \triangleq \{\boldsymbol{x} : g(\boldsymbol{x}) < \eta\}$. More details about the Switch Model (33)-(43) and a pseudocode are given in [25].

2.4. Stick-slip behavior

In this section we consider the stick-slip behavior of the bristle model (13) by investigating the existence of a stable limit cycle when the bristle model is used to represent the friction force in the system (18)-(20) shown in Figure 2 with the vertical motion described by (21)-(22).

We use the Switch Model (33)-(43) to simulate the system (18)-(22) with friction force defined by (13). The system (18)-(22) can be formulated as the differential inclusion (32) with $\boldsymbol{x} = \begin{bmatrix} x & v & l & y & \dot{y} \end{bmatrix}^{\mathrm{T}}$, the set Σ defined by the roots of the function $g(\boldsymbol{x}) = v$, the normal to Σ defined by $\boldsymbol{n} \triangleq \nabla g(\boldsymbol{x}) =$

$\begin{bmatrix} 0 & 1 & 0 & 0 & 0 \end{bmatrix}^{\mathrm{T}}$, and the vector fields $\boldsymbol{f}_+(\boldsymbol{x})$ and $\boldsymbol{f}_-(\boldsymbol{x})$ defined as

$$\boldsymbol{f}_+(\boldsymbol{x}) \triangleq \begin{bmatrix} v \\ \frac{1}{m}(Kl - F_{f+}(x,y)) \\ v_p - v \\ \dot{y} \\ -mg + F_{y+}(x,y) \end{bmatrix}, \tag{44}$$

$$\boldsymbol{f}_-(\boldsymbol{x}) \triangleq \begin{bmatrix} v \\ \frac{1}{m}(Kl - F_{f-}(x,y)) \\ v_p - v \\ \dot{y} \\ -mg + F_{y-}(x,y) \end{bmatrix}, \tag{45}$$

where $F_{f+}(x,y)$ and $F_{f-}(x,y)$ are defined by (10) and (12), respectively, and

$$F_{y+}(x,y) \triangleq F_{ys+}(x,y) + F_{yb}(y), \tag{46}$$

$$F_{y-}(x,y) \triangleq F_{ys-}(x,y) + F_{yb}(y), \tag{47}$$

where $F_{ys+}(x,y)$ is defined by (15) and $F_{ys-}(x,y)$ by (16).

Figure 4(a) shows the projection of the trajectories of (44)-(45) onto the l-v plane, obtained by using the Switch Model (33)-(43), with parameter values $m = 1$ kg, $w = 1$ m, $d = 2$ m, $\alpha = 15°$, $K = 5$ N/m, $N = 500$, $k = 0.01$ N/m, $h_0 = 2.69$ m, $\eta = 10^{-6}$, and $v_p = 0.1$ m/s. In this plane, the trajectory converges to a stable limit cycle that includes a line segment on which the motion is given by $v = 0$ and $\dot{l} = v_p$. This segment corresponds to the "stick" phase, during which the body is stationary. The "slip" phase corresponds to the curved part of the limit cycle for which $v \neq 0$. The time histories of the spring length, velocity, height, and position of the body are shown in Figure 4(b). Note that the velocity is characterized by segments in which the velocity is zero and segments in which velocity quickly increases. This behavior is typical for stick-slip motion.

The time history of the friction force and plots of the friction force versus height y and versus velocity v are shown in Figure 5. This figure also shows the relationship between the height y and velocity v. The friction force is a decreasing function of height, which is consistent with the experimental results presented in [2, 4, 5] as well as the expression (13). In the bristle model, as the height increases, compression of the bristles from their relaxed

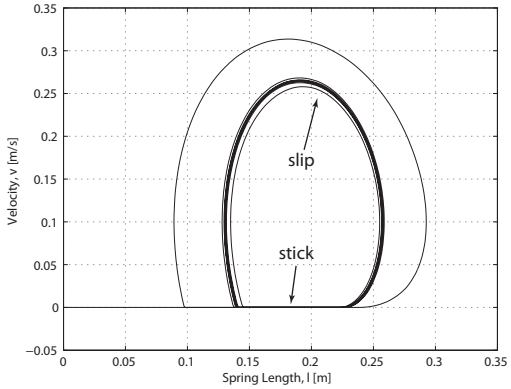

(a)

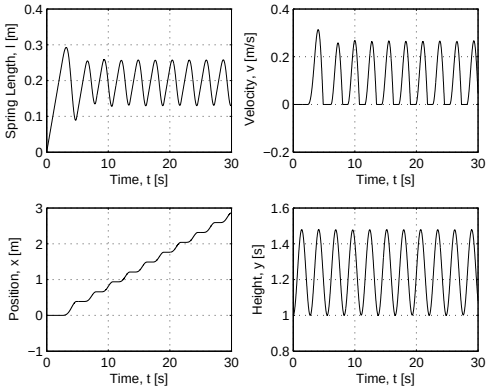

(b)

Figure 4: The stick-slip limit cycle and time histories of the spring length l, velocity v, position x, and height y for the system (44)-(45) with F_f modeled by (13). (a) shows the limit cycle and (b) shows the time histories of the states. The trajectories projected onto the l-v plane form a stable limit cycle.

length h_0 decreases. Thus, the friction force decreases also. Furthermore, the friction force decreases as the velocity increases. The velocity/friction-force curve forms a loop, which we refer to as the *dynamic Stribeck effect*. The height versus velocity plot in Figure 5 shows that the velocity increases with height. That is, the body moves higher as it speeds up, and it moves lower as it slows down. This is planing.

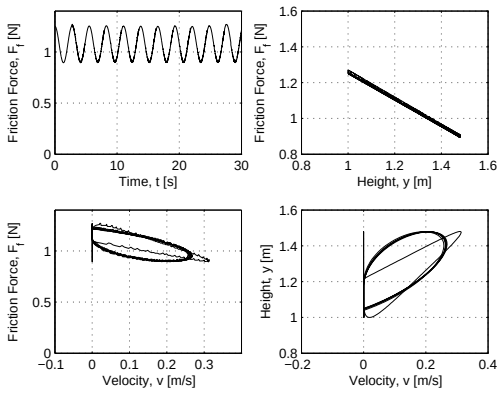

Figure 5: The friction force of the compressed bristle model. The figure shows the dependence of the friction force on time t, height y, and velocity v. The lower left plot shows the dynamic Stribeck effect, while the lower right plot shows the velocity-height curve.

2.5. Physical mechanism that leads to the dynamic Stribeck effect

In the vertical direction, the system consisting of the body and the bristles described by (21)-(22) represents an undamped oscillator. Thus, if the body is initially not in a vertical equilibrium or if it is slightly disturbed from an equilibrium position, then it oscillates vertically whether or not it is moving horizontally. Since the friction force (13) depends linearly on the height y through $h_i(x, v, y)$, the vertical oscillation of the body results in oscillation of the magnitude of the friction force F_f defined by (13). The oscillations in F_f are visible in Figure 5. The horizontal velocity increases with y because the friction force F_f decreases as y increases, and thus the horizontal acceleration of the body increases. The opposite happens when y decreases.

Furthermore, as seen in Figure 5, the drop in the friction force that occurs when a single bristle transitions from contacting the slanted surface of the body to contacting the horizontal surface of the body is small compared to the amplitude of oscillation of the friction force due to vertical oscillation of the body. As the amplitude of the vertical oscillation of the body decreases, the change in friction force due to a bristle transition from contacting the slanted surface of the body to contacting the horizontal surface of the body becomes the mechanism that leads to stick-slip. In comparison with the discontinuous rotating bristle model [19, 20], the individual bristles do not have a visible effect on the stick-slip behavior or the dynamic Stribeck effect of the compressed bristle model.

To demonstrate, we simulate (18)-(20) with the friction force (13). However, in the vertical direction we assume that the body oscillates according to $y(t) = A\sin(\omega t)$. We use the Switch Model (33)-(43), and reformulate (18)-(20) as a differential inclusion with $\boldsymbol{f}_+$ and $\boldsymbol{f}_-$ defined by

$$\boldsymbol{f}_+(\boldsymbol{x}) \triangleq \begin{bmatrix} v \\ \frac{1}{m}(Kl - F_{f+}(x,y)) \\ v_p - v \end{bmatrix}, \tag{48}$$

$$\boldsymbol{f}_-(\boldsymbol{x}) \triangleq \begin{bmatrix} v \\ \frac{1}{m}(Kl - F_{f-}(x,y)) \\ v_p - v \end{bmatrix}, \tag{49}$$

where $F_{f+}(x,y)$ is defined by (10) and $F_{f-}(x,y)$ is defined by (12).

The results are shown in Figure 6 for $A = 0.3$ m and $A = 1.3$ m and for $\omega = 6.8$ rad/s. This frequency of oscillation is approximately equal to the natural frequency of the vertical oscillations of the body shown in Figure 4(b). The parameter values used are $m = 1$ kg, $K = 2$ N/m, $w = 1$ m, $d = 2$ m, $\alpha = 15°$, $N = 100$, $k = 0.05$ N/m, and $h_0 = 4.46$ m. Note that the dynamic Stribeck effect as well as the dependence of velocity on the height y of the body are more prominent for larger values of A. Also, once the body begins moving horizontally, the friction force becomes less smooth, that is, there are small drops in the friction force that correspond to the transition of a bristle from contacting the slanted surface of the body to contacting the horizontal surface of the body.

2.6. Hysteresis map

In this section we analyze the input-output properties of the bristle model. We consider the mass-spring configuration shown in Figure 3 and described by (21)-(27). We use the Switch Model (33)-(43) to smooth out the discontinuity in the bristle model friction force (13).

The system (21)-(27) can be formulated as a differential inclusion (32) with $\boldsymbol{x} = \begin{bmatrix} x & v & y & \dot{y} \end{bmatrix}^{\mathrm{T}}$, the set Σ defined by the roots of function $g(\boldsymbol{x}) = v$, the normal to Σ defined by $\boldsymbol{n} \triangleq \nabla g(\boldsymbol{x}) = \begin{bmatrix} 0 & 1 & 0 & 0 \end{bmatrix}^{\mathrm{T}}$, and vector

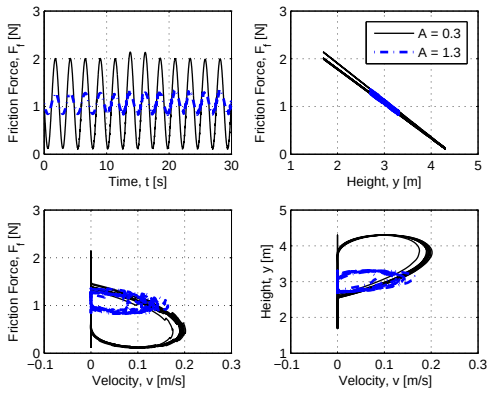

Figure 6: Simulations of (44)-(45) with the prescribed height trajectory $y(t) = A\sin(\omega t)$, where $A = 0.3$ m and $A = 1.3$ m and for $\omega = 6.8$ rad/s and F_f modeled by (13). The dynamic Stribeck effect can be seen in the lower left plot. This effect is more pronounced for the vertical oscillation with the larger amplitude.

fields $\boldsymbol{f}_+(\boldsymbol{x})$ and $\boldsymbol{f}_-(\boldsymbol{x})$ defined as

$$\boldsymbol{f}_+(\boldsymbol{x}) \triangleq \begin{bmatrix} v \\ \frac{1}{m}(-Kx + u - F_{f+}(x,y)) \\ \dot{y} \\ -mg + F_{y+}(x,y) \end{bmatrix}, \tag{50}$$

$$\boldsymbol{f}_-(\boldsymbol{x}) \triangleq \begin{bmatrix} v \\ \frac{1}{m}(-Kx + u - F_{f-}(x,y)) \\ \dot{y} \\ -mg + F_{y-}(x,y) \end{bmatrix}, \tag{51}$$

where $F_{f+}(x,y)$ and $F_{f-}(x,y)$ are defined by (10) and (12), respectively, and $F_{y+}(x,y)$ and $F_{y-}(x,y)$ are defined by (46) and (47), respectively.

The input-output map of (50)-(51), obtained from the Switch Model (33)-(43), with parameter values $m = 1$ kg, $K = 2$ N/m, $w = 1$ m, $d = 2$ m, $\alpha = 15^\circ$, $g = 10$ m/s^2, $N = 500$, $\Delta = 0.0035$ m, $h_0 = 1.65$ m, $k = 0.01$ N/m, $\eta = 10^{-6}$, and $u(t) = 2\sin(0.01t)$ N is shown in Figure 7(a). The time histories of the states and the friction force are shown in Figure 7(b). Since the plot of the input $u(t)$ versus position of the body x forms a loop at a low frequency of the input, the system (50)-(51) with friction force described by (13) is hysteretic [18]. During the motion, the energy is stored

in the bristles and dissipated by the oscillation of the bristles once the mass passes over them. The energy dissipation is manifested in the force-position hysteresis loop, whose area 2.384 J is equal to the amount of dissipated energy. Note that the hysteresis map has a staircase shape typical of stick-slip motion. Furthermore the time history of the velocity shows jumps in the velocity, which means that the body goes through periods of sticking, where the velocity is zero, followed by slipping, where the velocity is nonzero.

The plots in Figure 8 show the height and velocity versus the friction force. In accordance with [4] the magnitude of the friction force decreases with height. Furthermore, the magnitude of the friction force drops with an increase in velocity, and the friction force-velocity curve forms a loop as shown in Figure 8, which indicates the presence of the dynamic Stribeck effect.

3. Simplified Bristle Model

In this section we introduce a simplified version of the bristle model, which eliminates the need for the Switch Model. The simplified bristle model (SBM) is a single-state model [3, 27–29] that captures the stick-slip properties and the characteristics of the friction force-height, friction force-velocity, and velocity-height relationships of the compressed bristle model.

3.1. Single-state friction models

Single-state friction models such as the Dahl and LuGre model involve a state variable z that represents the internal friction mechanism. These models have the form

$$\dot{z} = v\left(1 - \alpha(v,z)\text{sign}(v)\frac{z}{z_{ss}(v)}\right), \tag{52}$$

$$F_f = \sigma_0 z + \sigma_1 \dot{z} + \sigma_2 v, \tag{53}$$

where σ_0, σ_1, σ_2 are positive constants, z is the internal friction state, $z_{ss}(v)$ determines the shape of the steady-state z curve, and F_f is the friction force. The function $\alpha(v,z)$ determines the presence and type of elastoplastic presliding displacement [27, 28]. For simplicity, we set $\alpha(v,z) = 1$ and rewrite

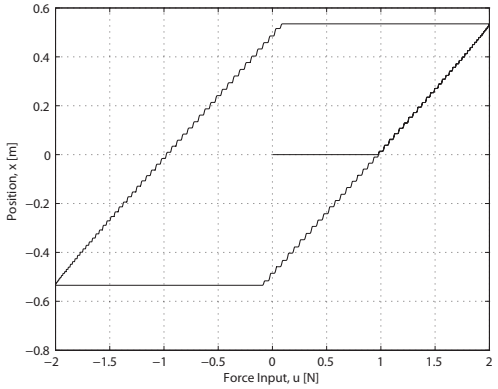

(a)

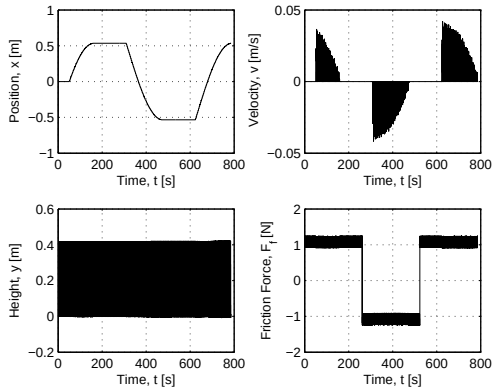

(b)

Figure 7: The input-output map and time histories of the position x, velocity v, height y, and friction force F_f of the mass-spring system shown in Figure 3 with the friction force modeled by (13). The input-output map is hysteretic due to the energy dissipated in order to compress the bristle springs. The energy dissipated is equal to the area of the hysteresis map.

(52)-(53) as

$$\dot{z} = v - \frac{|v|}{z_{ss}(v)} z, \tag{54}$$

$$F_f = \sigma_0 z + \sigma_1 \dot{z} + \sigma_2 v. \tag{55}$$

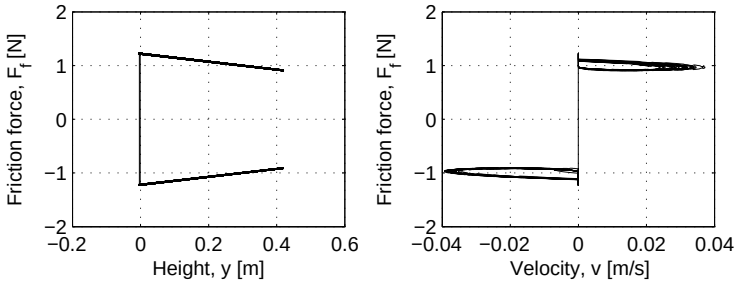

Figure 8: Dependence of friction force on height and velocity. The magnitude of the friction force decreases with increasing height and velocity. The drop in friction force with increased velocity is the Stribeck effect.

Setting $z_{ss}(v)$ to be

$$z_{ss}(v) = \frac{1}{\sigma_0}\left(F_c + (F_s - F_c)e^{-(v/v_s)^2}\right), \tag{56}$$

where F_c, F_s, and v_s are constants, yields the LuGre model [10, 11], which exhibits stick-slip, hysteresis, and the Stribeck effect.

In steady-state motion, $\dot{z} = 0$, and thus $z = \text{sign}(v)z_{ss}(v)$. Furthermore, if $\sigma_1 = \sigma_2 = 0$, then

$$F_f = \sigma_0 z = \text{sign}(v)\sigma_0 z_{ss}(v). \tag{57}$$

3.2. Mean friction force

The goal in formulating the SBM is to capture the characteristics of the friction force-height, friction force-velocity, and velocity-height relationships of the bristle model, while redefining the bristle model equations as a continuous model. As shown in Figure 5, the friction force-velocity and height-velocity curves form loops. To model these loops, we fit a function to the mean values of each loop and then reformulate the compressed bristle model equations in the form of a single-state friction model.

First, we find the mean value of the friction force as a function of height y. For all $v \geq 0$, the bristle height $h_{i+}(x, y)$ is calculated from (2), and the ith bristle contributes to the friction force if $x_{b_i} \in \mathcal{X}_{b+}(x)$ defined by (7), that

is,

$$x + \frac{d}{2} - d_1 \leq x_{b_i} \leq x + \frac{d}{2}. \tag{58}$$

Thus, over all relevant values of x_{b_i}, $h_{i+}(x, y)$ takes on the maximum and minimum values

$$h_{i+,\max}(x, y) = y - \frac{w}{2} + \frac{w}{d_2}\left(x + \frac{d}{2} - d_1 - \left(x + \frac{d}{2} - d_1\right)\right) = y - \frac{w}{2}, \tag{59}$$

$$h_{i-,\min}(x, y) = y - \frac{w}{2} + \frac{w}{d_2}\left(x + \frac{d}{2} - \left(x + \frac{d}{2} - d_1\right)\right) = y + \frac{w}{2}. \tag{60}$$

Similarly, for all $v < 0$, the bristle height $h_{i-}(x)$ is found from (3), and the ith bristle contributes to the friction force if $x_{b_i} \in \mathcal{X}_{b-}(x)$ defined by (8), that is,

$$x - \frac{d}{2} \leq x_{b_i} \leq x - \frac{d}{2} + d_1. \tag{61}$$

Thus, over all relevant values of x_{b_i}, $h_{i-}(x, y)$ takes on the maximum and minimum values

$$h_{i-,\max}(x, y) = y - \frac{w}{2} + \frac{w}{d}\left(x - \frac{d}{2} + d_1 - \left(x - \frac{d}{2} + d_1\right)\right) = y - \frac{w}{2}, \tag{62}$$

$$h_{i-,\min}(x, y) = y - \frac{w}{2} + \frac{w}{d}\left(x - \frac{d}{2} + d_1 - \left(x - \frac{d}{2}\right)\right) = y + \frac{w}{2}. \tag{63}$$

Thus, for all $v \in \mathbb{R}$, the mean value of the ith bristle height $h_i(x, v, y)$ is

$$\overline{h_i}(y) = \frac{1}{2}\left(y + \frac{w}{2} + y - \frac{w}{2}\right) = y, \tag{64}$$

and the mean value of the friction force is

$$\overline{F_f}(x, v, y) = \begin{cases} k\cos(\alpha)\sum_{i=1}^{n_+} \overline{h_0 - h_i} = n_+ k\cos(\alpha)(\overline{h_0 - h_i}), \text{ if } v \geq 0, \\ -k\cos(\alpha)\sum_{i=1}^{n_-} \overline{h_0 - h_i} = -n_- k\cos(\alpha)(\overline{h_0 - h_i}), \text{ if } v < 0. \end{cases} \tag{65}$$

where $\overline{h_0 - h_i}$ denotes the mean value of $h_0 - h_i$. To find $\overline{h_0 - h_i}$, we use

$$\overline{h_0 - h_i} = \frac{\sum_{i=1}^{n}(h_0 - h_i)}{n} = h_0 - \frac{\sum_{i=1}^{n} h_i}{n} = h_0 - \overline{h_i} = h_0 - y, \tag{66}$$

so that

$$\overline{F_f}(y, v) = \text{sign}(v) kn \cos(\alpha)(h_0 - y) = \text{sign}(v)\tilde{k}(h_0 - y), \tag{67}$$

where $\tilde{k} = kn\cos(\alpha)$ and we assume that $n_+ = n_- = n$. Equation (67) describes the friction force as a function of height.

3.3. Velocity-height curve fits

In order to obtain an expression for friction force as a function of velocity we now formulate the height y as a function of velocity v. We can then use $y(v)$ in (67) to obtain $F_f(v)$.

Instead of a function that approximates the velocity-height loop, we find a function that approximates the mean value of y as a function of velocity. The actual and mean values of the height y shown in Figure 9 are obtained from simulating (44)-(45) with the Switch Model (33)-(43) and parameters $m = 1$ kg, $K = 5$ N/m, $w = 1$ m, $d = 2$ m, $\alpha = 15°$, $g = 10$ m/s^2, $N = 500$, $k = 0.01$ N/m, $\Delta = 0.0035$ m, $h_0 = 1.65$ m, $\eta = 10^{-6}$, and $v_p = \pm 0.1$ m/s. Note that y is limited to the range $0 \leq y \leq h_0$ since the bristles do not stretch beyond their relaxed length h_0 or compress beyond the level of the ground.

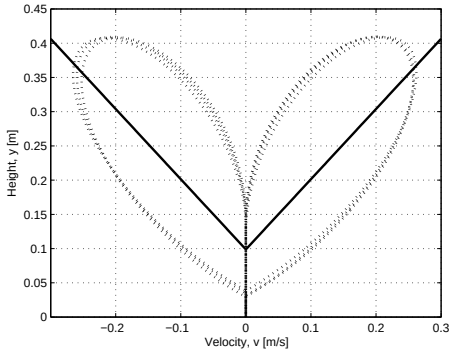

Figure 9: The velocity-height curve and its mean value. The mean value is shown by the solid line, and the simulation result is shown by the dashed line.

To approximate the mean value of the velocity-height curve, we choose two different functions, namely, hyperbolic secant and exponential. The hyperbolic secant expression is

$$\overline{y}(v) = y_1 - y_2 \text{sech}\left(\frac{v}{v_s}\right), \tag{68}$$

where y_1 and y_2 determine the maximum and minimum values of $\overline{y}$ and v_s is the velocity at which the height increases from y_1 to y_2. If $\overline{y}(v)$ is defined by (68), then the approximation of the mean friction force is

$$\overline{F_f}(v) = \text{sign}(v)\tilde{k}\left(h_0 - y_1 + y_2 \text{sech}\left(\frac{v}{v_s}\right)\right). \tag{69}$$

Figure 10(a) shows the approximation of the mean height $\overline{y}$ as the function of velocity defined by (68), while Figure 10(b) shows the approximation of the mean friction force $\overline{F_f}$ as the function of velocity defined by (69) with the parameter values $y_1 = 0.4$ m, $y_2 = 0.3$ m, $v_s = \frac{0.6}{2\pi}$ m/s, $\tilde{k} = 0.75$ N/m, and $h_0 = 1.64$ m. Figure 10 also shows the actual and mean values of the height y and the friction force F_f obtained from simulating (44)-(45) with parameters $m = 1$ kg, $K = 5$ N/m, $w = 1$ m, $d = 2$ m, $\alpha = 15^\circ$, $g = 10$ m/s^2, $N = 500$, $k = 0.01$ N/m, $\Delta = 0.0035$ m, $h_0 = 1.65$ m, $\eta = 10^{-6}$, and $v_p = \pm 0.1$ m/s

Alternatively, we can approximate the mean height by the exponential function of velocity

$$\overline{y}(v) = y_1 - y_2 e^{-(v/v_s)^2}, \tag{70}$$

where y_1 and y_2 are the maximum and minimum values of mean height, respectively, and v_s is the velocity at which the mean height increases from y_2 to y_1. If $\overline{y}$ is defined by (70), then the approximation of the mean friction force is

$$\overline{F_f}(v) = \text{sign}(v)\tilde{k}\left(h_0 - y_1 + y_2 e^{-(v/v_s)^2}\right). \tag{71}$$

Figure 11(a) shows the approximation of the mean height $\overline{y}$ as the function of velocity defined by (70), while Figure 11(b) shows the approximation of the mean friction force $\overline{F_f}$ as the function of velocity defined by (71) with parameters $y_1 = 0.4$ m, $y_2 = 0.3$ m, $v_s = 0.1$ m/s, $\tilde{k} = 0.75$ N/m, and

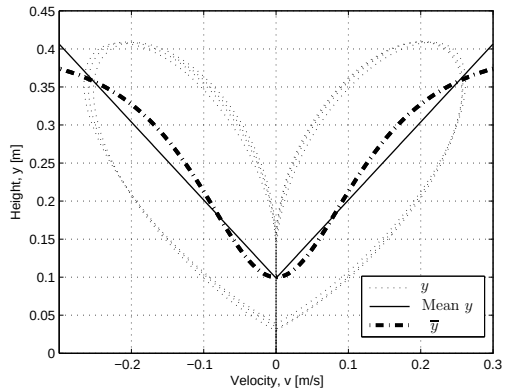

(a)

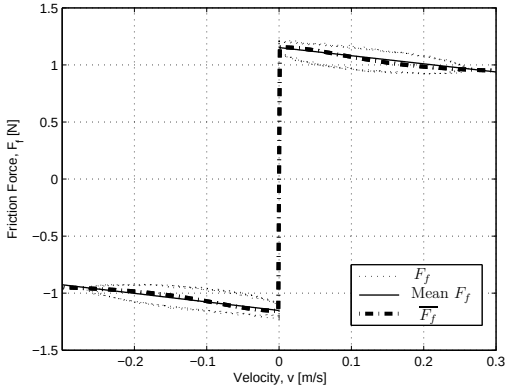

(b)

Figure 10: Approximation of the mean height (68) and mean friction force (69) of the SBM friction model (dash-dot) obtained by approximating the mean height by the hyperbolic secant function of velocity. (a) shows the approximation of the mean height $\overline{y}$ as the function of velocity defined by (68), while (b) shows the approximation of the mean friction force $\overline{F_f}$ as the function of velocity defined by (69). The actual and mean values of the height y and friction force F_f are also shown by the dotted and solid lines, respectively.

$h_0 = 1.7$ m. Figure 10 also shows the actual and mean values of the height y and the friction force F_f obtained from simulating (44)-(45) with parameters $m = 1$ kg, $K = 5$ N/m, $w = 1$ m, $d = 2$ m, $\alpha = 15^\circ$, $g = 10$ m/s^2, $N = 500$, $k = 0.01$ N/m, $\Delta = 0.0035$ m, $h_0 = 1.65$ m, $\eta = 10^{-6}$, and $v_p = \pm 0.1$ m/s

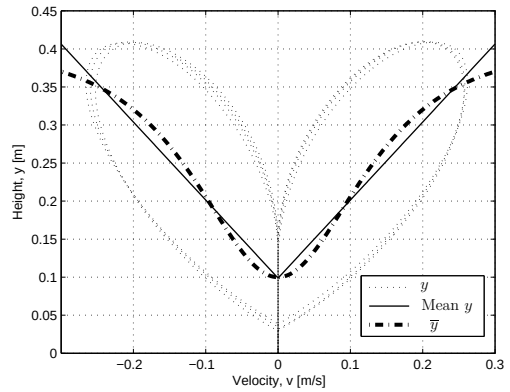

(a)

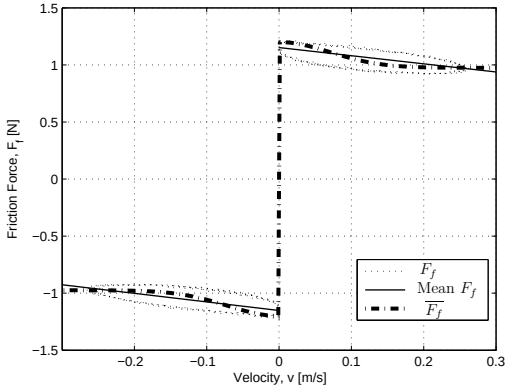

(b)

Figure 11: Approximation of the mean height (70) and mean friction force (71) of the SBM friction model (dash-dot) obtained by approximating the mean height by an exponential function of velocity with parameters $y_1 = 1$ m, $y_2 = 0.5$ m, $v_s = 0.1$ m/s, $\tilde{k} = 1$ N/m, and $h_0 = 2$ m. (a) shows the approximation of the mean height $\overline{y}$ as the function of velocity defined by (70), (b) shows the approximation of the mean friction force $\overline{F_f}$ as the function of velocity defined by (71). The actual and mean values of the height y and friction force F_f are also shown by the dotted and solid lines, respectively.

Combining (57) and (69) yields

$$z_{ss}(v) = \frac{\tilde{k}}{\sigma_0}\left(h_0 - y_1 + y_2 \text{sech}\left(\frac{v}{v_s}\right)\right), \tag{72}$$

and the single-state friction model

$$\dot{z} = v - \sigma_0 \frac{|v|}{\tilde{k}\left(h_0 - h_1 + h_2 \text{sech}\left(\frac{v}{v_s}\right)\right)} z, \tag{73}$$

$$F_f = \sigma_0 z. \tag{74}$$

Furthermore, combining (57) and (71) gives the alternative expression

$$z_{ss} = \frac{\tilde{k}}{\sigma_0}\left(h_0 - y_1 + y_2 e^{-(v/v_s)^2}\right), \tag{75}$$

and the alternative single-state friction model

$$\dot{z} = v - \sigma_0 \frac{|v|}{\tilde{k}\left(h_0 - y_1 + y_2 e^{-(v/v_s)^2}\right)} z, \tag{76}$$

$$F_f = \sigma_0 z. \tag{77}$$

The equations (76)-(77) are identical to the LuGre equations (54)-(56) with $\sigma_1 = \sigma_2 = 0$, $\tilde{k}(h_0 - y_1) = F_c$, and $\tilde{k}y_2 = F_s - F_c$. In order to further demonstrate the similarity of the LuGre model and the simplified bristle model, we simulate the systems of equations (18)-(20) and (26)-(27) with the friction force (76)-(77). The output of the system (18)-(20) with the friction force (76)-(77) and input velocity $v_p = 0.1$ m/s is shown in Figure 12(a). The parameter values are $m = 1$ kg, $K = 1$ N/m, $y_1 = 1$ m, $y_2 = 0.5$ m, $v_s = 0.1$ m/s, $\tilde{k} = 1$ N/m, $\sigma = 10^5$, and $h_0 = 2$ m. The results of simulating (26)-(27) with the friction force (76)-(77) and input defined by $u(t) = 5\sin(0.01t)$ N, are shown in Figure 12(b). The stick-slip behavior is visible in both simulations, and the system is hysteretic as shown by the hysteretic input-output map.

4. Conclusions

In this paper we developed the compressed bristle model, an asperity-based friction model in which the friction force arises through the frictionless and lossless interaction of a body with an endless row of bristles that represent the microscopic roughness of the contacting surfaces. The bristles consist of a frictionless roller attached to the ground through a spring. The body is allowed to move horizontally and vertically over the bristles, which are com-

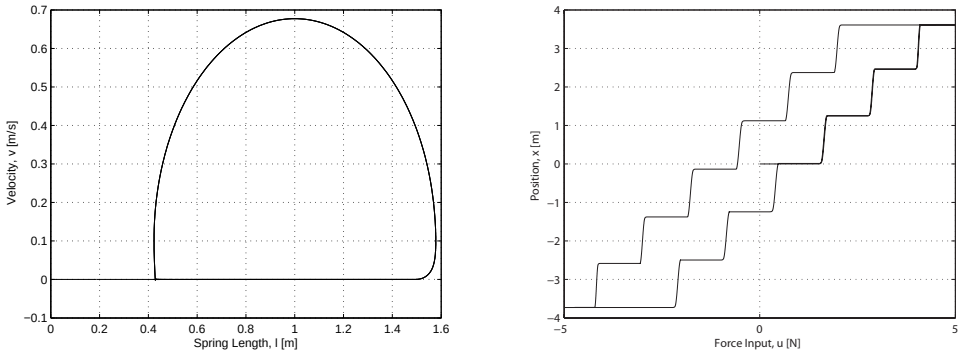

(a) (b)

Figure 12: The stick-slip limit cycle of (18)-(20) and the hysteresis map of (26)-(27) with friction force modeled by (76)-(77). The stick-slip limit cycle in the l-v plane is shown in (a). (b) shows the hysteresis map with staircase shape typical of stick-slip motion.

pressed and thus apply a reaction force at the point of contact. The friction force is the sum of all horizontal components of the contact forces between all of the bristles and the body. As the body passes over the compressed bristles, they are suddenly released, and the energy stored in each spring is dissipated by viscous dashpot regardless of how slowly the body moves. Thus, energy is dissipated in the limit of DC operation and the system is hysteretic.

In the vertical direction, the body and the bristles form an undamped oscillator. The body oscillates vertically regardless of whether it is moving horizontally or not. During the vertical oscillations, as the body rises, the friction force decreases, and the body speeds up. This mechanism gives rise to the dynamic Stribeck effect, which refers to the fact that the friction force-velocity curve forms a loop.

Furthermore, we showed that the compressed bristle model exhibits stick-slip friction and that the bristle model equations can be simplified to give a single-state friction model. The simplified bristle model (SBM) retains the stick-slip and hysteresis properties of the original model. The internal friction state of the SBM can be interpreted as the average deflection of the bristles from their relaxed length. The simplified bristle model is equivalent to the LuGre model.

5. Acknowledgments

This research was made with Government support under and awarded by DoD, Air Force Office of Scientific Research, National Defense Science and Engineering Graduate (NDSEG) Fellowship, 32 CFR 168a and NSF grant 0758363.

References

[1] B. Armstrong-Hélouvry, Control of Machines with Friction, Kluwer, Boston, MA, 1991.

[2] B. Armstrong-Hélouvry, P. Dupont, C. Canudas de Wit, A survey of models, analysis tools and compensation methods for the control of machines with friction, Automatica 30 (1994) 1083–1138.

[3] J. J. Choi, S. I. Han, J. S. Kim, Development of a novel dynamic friction model and precise tracking control using adaptive back-stepping sliding mode controller, Mechatronics 16 (2006) 97–104.

[4] D. M. Tolstoi, Significance of the normal degree of freedom and natural normal vibrations in contact friction, Wear 10 (1967) 199–213.

[5] T. Sakamoto, Normal displacement and dynamic friction characteristics in a stick-slip process, Tribology International 20 (1987) 25–31.

[6] J. A. C. Martins, J. T. Oden, F. M. F. Simoes, Recent advances in engineering science: A study of static and kinetic friction, Int. J. Engng. Sci. 28 (1990) 29–92.

[7] C. Canudas de Wit, H. Olsson, K. J. Åström, P. Lischinsky, A new model for control of systems with friction, IEEE Trans. Autom. Contr. 40 (1995) 419–425.

[8] H. Olsson, K. J. Åström, C. Canudas de Wit, M. Gafvert, P. Lischinsky, Friction models and friction compensation, European Journal of Control 4 (1998) 176–195.

[9] N. Barabanov, R. Ortega, Necessary and sufficient conditions for passivity of the LuGre friction model, IEEE Trans. Autom. Contr. 45 (2000) 675–686.

[10] F. Avanzini, S. Serafin, D. Rocchesso, Modeling interaction between rubbed dry surfaces using an elasto-plastic friction model, in: Proc. 5^{th} Int. Conference on Digital Audio Effects, Hamburg, Germany, pp. 111–116.

[11] K. J. Astrom, C. Canudas de Wit, Revisiting the LuGre friction model, IEEE Control Systems Magazine 28 (2008) 101–114.

[12] A. K. Padthe, N. A. Chaturvedi, D. S. Bernstein, S. P. Bhat, A. M. Waas, Feedback stabilization of snap-through buckling in a preloaded two-bar linkage with hysteresis, Int. J. Non-Linear Mech. 43 (2008) 277–291.

[13] A. K. Padthe, B. Drincic, J. Oh, D. D. Rizos, S. D. Fassois, D. S. Bernstein, Duhem modeling of friction-induced hysteresis: Experimental determination of gearbox stiction, IEEE Contr. Sys. Mag. 28 (2008) 90–107.

[14] D. A. Haessig, B. Friedland, On the modeling and simulation of friction, ASME J. Dyn. Sys. Meas. Contr. 113 (1991) 354–361.

[15] N. E. Dowling, Mechanical Behavior of Materials: Engineering Methods for Deformation, Fracture, and Fatigue, Prentice Hall, Englewood Cliffs, NJ, 1993.

[16] F. Al-Bender, V. Lampert, J. Swevers, A novel generic model at asperity level for dry friction force dynamics, Tribology Letters 16 (2004) 81–93.

[17] F. Al-Bender, J. Swevers, Characterization of friction force dynamics: Behavior and modeling on micro and macro scales, IEEE Contr. Sys. Mag. 28 (2008) 82–91.

[18] J. Oh, D. S. Bernstein, Semilinear Duhem model for rate-independent and rate-dependent hysteresis, IEEE Trans. Autom. Contr. 50 (2005) 631–645.

[19] B. Drinčić, D. S. Bernstein, A sudden-release bristle model that exhibits hysteresis and stick-slip friction, in: Proc. Amer. Contr. Conf., San Francisco, CA, pp. 2456–2461.

[20] B. Drinčić, D. S. Bernstein, A frictionless bristle-based friction model that exhibits hysteresis and stick-slip behavior, J. Sound and Vibration (2012). Submitted.

[21] W. B. Horne, R. C. Dreher, Phenomena of Pneumatic Tire Hydroplaning, Technical Note TN D-2056, NASA, 1963.

[22] P. Andren, A. Jolkin, Elastohydrodynamic aspects on the tyre-pavement contact at aquaplaning, VTI rapport 483A, Swedish National Road and Transport Research Institute, 2003. Http://www.mobilidades.org/arquivo/aquaplanning.pdf.

[23] A. J. Tuononen, M. J. Matilainen, Real-time estimation of aquaplaning with an optical tyre sensor, Institution of Mechanical Engineers, Part D: J. Automobile Engineering 223 (2009) 1263–1272.

[24] R. I. Leine, D. H. V. Campen, A. De Kraker, L. Van Den Steen, Stick-slip vibrations induced by alternate friction models, Nonlinear Dynamics 16 (1998) 41–45.

[25] R. I. Leine, H. Nijmeijer, Dynamics and Bifurcations of Non-smooth Mechanical Systems, Springer, Berlin, 2004.

[26] A. F. Filippov, Differential Equations with Discontinuous Righthand Sides, Kluwer Academic Publishers, Dordrecht, The Netherlands, 1988.

[27] P. Dupont, B. Armstrong, V. Hayward, Elasto-plastic friction model: Contact compliance and stiction, in: Proc. Amer. Contr. Conf., Chicago, IL, pp. 1072–1077.

[28] P. Dupont, V. Hayward, B. Armstrong, F. Altpeter, Single state elasto-plastic friction models, IEEE Trans. Autom. Contr. 47 (2002) 787–792.

[29] B. S. R. Armstrong, Q. Chen, The z-properties chart: Visualizing the presliding behavior of state-variable friction models, IEEE Control Systems Magazine 28 (2008) 79–89.